Nuclear matter effects on inline-formula> mml:math>mml:mrow>mml:mi>J/mml:mi>mml:mo>//mml:mo>mml:mi>ψ/mml:mi>/mml:mrow>/mml:math>/inline-formula> production in asymmetric Cu + Au collisions at inline-formula>mml:math>mml:mrow>mml:msqrt>mml:msub>mml:mi>s/mml:mi>mml:msub>mml:mrow/>mml:mrow>mml:mi>N/mml:mi>mml:mi>N/mml:mi>/mml:mrow>/mml:msub>/mml:msub>/mml:msqrt>mml:mo>=/mml:mo>mml:mn>200/mml:mn>/mml:mrow>/mml:math>/inline-formula> GeV/article-title>

A. Adare *et al.* (PHENIX Collaboration)

Phys. Rev. C **90**, 064908 — Published 18 December 2014

DOI: 10.1103/PhysRevC.90.064908

Nuclear matter effects on J/ψ production in asymmetric Cu+Au collisions at $\sqrt{s_{_{NN}}}$=200 GeV.

A. Adare,[13] C. Aidala,[37,41] N.N. Ajitanand,[55] Y. Akiba,[50,51] R. Akimoto,[12] J. Alexander,[55] M. Alfred,[22] K. Aoki,[50] N. Apadula,[27,56] Y. Aramaki,[50] H. Asano,[33,50] E.T. Atomssa,[56] T.C. Awes,[47] B. Azmoun,[7] V. Babintsev,[23] M. Bai,[6] X. Bai,[11] N.S. Bandara,[40] B. Bannier,[56] K.N. Barish,[8] S. Bathe,[5,51] V. Baublis,[49] C. Baumann,[7] S. Baumgart,[50] A. Bazilevsky,[7] M. Beaumier,[8] S. Beckman,[13] R. Belmont,[41,60] A. Berdnikov,[53] Y. Berdnikov,[53] X. Bing,[46] D. Black,[8] D.S. Blau,[32] J.S. Bok,[45] K. Boyle,[51] M.L. Brooks,[37] J. Bryslawskyj,[5] H. Buesching,[7] V. Bumazhnov,[23] S. Butsyk,[44] S. Campbell,[27] C.-H. Chen,[51] C.Y. Chi,[14] M. Chiu,[7] I.J. Choi,[24] J.B. Choi,[10] S. Choi,[54] P. Christiansen,[38] T. Chujo,[59] V. Cianciolo,[47] Z. Citron,[61] B.A. Cole,[14] N. Cronin,[42] N. Crossette,[42] M. Csanád,[16] T. Csörgő,[62] A. Datta,[44] M.S. Daugherity,[1] G. David,[7] K. DeBlasio,[44] K. Dehmelt,[56] A. Denisov,[23] A. Deshpande,[51,56] E.J. Desmond,[7] L. Ding,[27] A. Dion,[56] J.H. Do,[63] O. Drapier,[34] A. Drees,[56] K.A. Drees,[6] J.M. Durham,[37] A. Durum,[23] L. D'Orazio,[39] T. Engelmore,[14] A. Enokizono,[50,52] H. En'yo,[50] S. Esumi,[59] K.O. Eyser,[7] B. Fadem,[42] N. Feege,[56] D.E. Fields,[44] M. Finger,[9] M. Finger, Jr.,[9] F. Fleuret,[34] S.L. Fokin,[32] J.E. Frantz,[46] A. Franz,[7] A.D. Frawley,[18] Y. Fukao,[30] K. Gainey,[1] C. Gal,[56] P. Gallus,[15] P. Garg,[3] A. Garishvili,[57] I. Garishvili,[36] H. Ge,[56] F. Giordano,[24] A. Glenn,[36] X. Gong,[55] M. Gonin,[34] Y. Goto,[50,51] R. Granier de Cassagnac,[34] N. Grau,[2] S.V. Greene,[60] M. Grosse Perdekamp,[24] Y. Gu,[55] T. Gunji,[12] H. Guragain,[19] T. Hachiya,[50] J.S. Haggerty,[7] K.I. Hahn,[17] H. Hamagaki,[12] S.Y. Han,[17] J. Hanks,[56] S. Hasegawa,[28] K. Hashimoto,[50,52] R. Hayano,[12] X. He,[19] T.K. Hemmick,[56] T. Hester,[8] J.C. Hill,[27] R.S. Hollis,[8] K. Homma,[21] B. Hong,[31] T. Hoshino,[21] J. Huang,[7,37] S. Huang,[60] T. Ichihara,[50,51] Y. Ikeda,[50] K. Imai,[28] Y. Imazu,[50] M. Inaba,[59] A. Iordanova,[8] D. Isenhower,[1] A. Isinhue,[42] D. Ivanishchev,[49] B.V. Jacak,[56] S.J. Jeon,[43] M. Jezghani,[19] J. Jia,[7,55] X. Jiang,[37] B.M. Johnson,[7] E. Joo,[31] K.S. Joo,[43] D. Jouan,[48] D.S. Jumper,[24] J. Kamin,[56] S. Kanda,[30] B.H. Kang,[20] J.H. Kang,[63] J.S. Kang,[20] J. Kapustinsky,[37] D. Kawall,[40] A.V. Kazantsev,[32] J.A. Key,[44] V. Khachatryan,[56] P.K. Khandai,[3] A. Khanzadeev,[49] K. Kihara,[59] K.M. Kijima,[21] C. Kim,[31] D.H. Kim,[17] D.J. Kim,[29] E.-J. Kim,[10] H.-J. Kim,[63] M. Kim,[54] Y.-J. Kim,[24] Y.K. Kim,[20] E. Kistenev,[7] J. Klatsky,[18] D. Kleinjan,[8] P. Kline,[56] T. Koblesky,[13] M. Kofarago,[16] B. Komkov,[49] J. Koster,[51] D. Kotchetkov,[46] D. Kotov,[49,53] F. Krizek,[29] K. Kurita,[52] M. Kurosawa,[50,51] Y. Kwon,[63] R. Lacey,[55] Y.S. Lai,[14] J.G. Lajoie,[27] A. Lebedev,[27] D.M. Lee,[37] G.H. Lee,[10] J. Lee,[17] K.B. Lee,[37] K.S. Lee,[31] S.H. Lee,[56] M.J. Leitch,[37] M. Leitgab,[24] B. Lewis,[56] X. Li,[11] S.H. Lim,[63] M.X. Liu,[37] D. Lynch,[7] C.F. Maguire,[60] Y.I. Makdisi,[6] M. Makek,[61,64] A. Manion,[56] V.I. Manko,[32] E. Mannel,[7] T. Maruyama,[28] M. McCumber,[13,37] P.L. McGaughey,[37] D. McGlinchey,[13,18] C. McKinney,[24] A. Meles,[45] M. Mendoza,[8] B. Meredith,[14,24] Y. Miake,[59] T. Mibe,[30] A.C. Mignerey,[39] A.J. Miller,[1] A. Milov,[61] D.K. Mishra,[4] J.T. Mitchell,[7] S. Miyasaka,[50,58] S. Mizuno,[50,59] A.K. Mohanty,[4] P. Montuenga,[24] T. Moon,[63] D.P. Morrison,[7,*] M. Moskowitz,[42] T.V. Moukhanova,[32] T. Murakami,[33,50] J. Murata,[50,52] A. Mwai,[55] T. Nagae,[33] S. Nagamiya,[30,50] J.L. Nagle,[13,†] M.I. Nagy,[16] I. Nakagawa,[50,51] H. Nakagomi,[50,59] Y. Nakamiya,[21] K.R. Nakamura,[33,50] T. Nakamura,[50] K. Nakano,[50,58] C. Nattrass,[57] P.K. Netrakanti,[4] M. Nihashi,[21,50] T. Niida,[59] R. Nouicer,[7,51] T. Novak,[62] N. Novitzky,[29] A.S. Nyanin,[32] E. O'Brien,[7] C.A. Ogilvie,[27] H. Oide,[12] K. Okada,[51] J.D. Orjuela Koop,[13] A. Oskarsson,[38] H. Ozaki,[59] K. Ozawa,[30] R. Pak,[7] V. Pantuev,[25] V. Papavassiliou,[45] I.H. Park,[17] S. Park,[54] S.K. Park,[31] S.F. Pate,[45] L. Patel,[19] M. Patel,[27] J.-C. Peng,[24] D.V. Perepelitsa,[7,14] G.D.N. Perera,[45] D.Yu. Peressounko,[32] J. Perry,[27] R. Petti,[56] C. Pinkenburg,[7] R. Pinson,[1] R.P. Pisani,[7] M.L. Purschke,[7] H. Qu,[1] J. Rak,[29] I. Ravinovich,[61] K.F. Read,[47,57] D. Reynolds,[55] V. Riabov,[49] Y. Riabov,[49,53] E. Richardson,[39] N. Riveli,[46] D. Roach,[60] S.D. Rolnick,[8] M. Rosati,[27] Z. Rowan,[5] J.G. Rubin,[41] M.S. Ryu,[20] B. Sahlmueller,[56] N. Saito,[30] T. Sakaguchi,[7] H. Sako,[28] V. Samsonov,[49] M. Sarsour,[19] S. Sato,[28] S. Sawada,[30] B. Schaefer,[60] B.K. Schmoll,[57] K. Sedgwick,[8] J. Seele,[51] R. Seidl,[50,51] Y. Sekiguchi,[12] A. Sen,[19,57] R. Seto,[8] P. Sett,[4] A. Sexton,[39] D. Sharma,[56] A. Shaver,[27] I. Shein,[23] T.-A. Shibata,[50,58] K. Shigaki,[21] M. Shimomura,[27] K. Shoji,[50] P. Shukla,[4] A. Sickles,[7] C.L. Silva,[37] D. Silvermyr,[47] B.K. Singh,[3] C.P. Singh,[3] V. Singh,[3] M. Skolnik,[42] M. Slunečka,[9] S. Solano,[42] R.A. Soltz,[36] W.E. Sondheim,[37] S.P. Sorensen,[57] M. Soumya,[55] I.V. Sourikova,[7] P.W. Stankus,[47] P. Steinberg,[7] E. Stenlund,[38] M. Stepanov,[40] A. Ster,[62] S.P. Stoll,[7] M.R. Stone,[13] T. Sugitate,[21] A. Sukhanov,[7] T. Sumita,[50] J. Sun,[56] J. Sziklai,[62] A. Takahara,[12] A. Taketani,[50,51] K. Tanida,[51,54] M.J. Tannenbaum,[7] S. Tarafdar,[3,61] A. Taranenko,[55] E. Tennant,[45] A. Timilsina,[27] T. Todoroki,[50,59] M. Tomášek,[15,26] H. Torii,[12] M. Towell,[1] R. Towell,[1] R.S. Towell,[1] I. Tserruya,[61] H.W. van Hecke,[37] M. Vargyas,[16,62] E. Vazquez-Zambrano,[14] A. Veicht,[14] J. Velkovska,[60] R. Vértesi,[62] M. Virius,[15] V. Vrba,[15,26] E. Vznuzdaev,[49] X.R. Wang,[45] D. Watanabe,[21] K. Watanabe,[50,52] Y. Watanabe,[50,51] Y.S. Watanabe,[30] F. Wei,[45] S. Whitaker,[27] S. Wolin,[24] C.L. Woody,[7] M. Wysocki,[47] B. Xia,[46] L. Xue,[19] S. Yalcin,[56] Y.L. Yamaguchi,[12] A. Yanovich,[23]

S. Yokkaichi,[50,51] I. Yoon,[54] Z. You,[37] I. Younus,[35,44] I.E. Yushmanov,[32] W.A. Zajc,[14] A. Zelenski,[6] and S. Zhou[11]
(PHENIX Collaboration)

[1]*Abilene Christian University, Abilene, Texas 79699, USA*
[2]*Department of Physics, Augustana College, Sioux Falls, South Dakota 57197, USA*
[3]*Department of Physics, Banaras Hindu University, Varanasi 221005, India*
[4]*Bhabha Atomic Research Centre, Bombay 400 085, India*
[5]*Baruch College, City University of New York, New York, New York, 10010 USA*
[6]*Collider-Accelerator Department, Brookhaven National Laboratory, Upton, New York 11973-5000, USA*
[7]*Physics Department, Brookhaven National Laboratory, Upton, New York 11973-5000, USA*
[8]*University of California - Riverside, Riverside, California 92521, USA*
[9]*Charles University, Ovocný trh 5, Praha 1, 116 36, Prague, Czech Republic*
[10]*Chonbuk National University, Jeonju, 561-756, Korea*
[11]*Science and Technology on Nuclear Data Laboratory, China Institute of Atomic Energy, Beijing 102413, People's Republic of China*
[12]*Center for Nuclear Study, Graduate School of Science, University of Tokyo, 7-3-1 Hongo, Bunkyo, Tokyo 113-0033, Japan*
[13]*University of Colorado, Boulder, Colorado 80309, USA*
[14]*Columbia University, New York, New York 10027 and Nevis Laboratories, Irvington, New York 10533, USA*
[15]*Czech Technical University, Zikova 4, 166 36 Prague 6, Czech Republic*
[16]*ELTE, Eötvös Loránd University, H-1117 Budapest, Pázmany Péter sétány 1/A, Hungary*
[17]*Ewha Womans University, Seoul 120-750, Korea*
[18]*Florida State University, Tallahassee, Florida 32306, USA*
[19]*Georgia State University, Atlanta, Georgia 30303, USA*
[20]*Hanyang University, Seoul 133-792, Korea*
[21]*Hiroshima University, Kagamiyama, Higashi-Hiroshima 739-8526, Japan*
[22]*Department of Physics and Astronomy, Howard University, Washington, DC 20059, USA*
[23]*IHEP Protvino, State Research Center of Russian Federation, Institute for High Energy Physics, Protvino, 142281, Russia*
[24]*University of Illinois at Urbana-Champaign, Urbana, Illinois 61801, USA*
[25]*Institute for Nuclear Research of the Russian Academy of Sciences, prospekt 60-letiya Oktyabrya 7a, Moscow 117312, Russia*
[26]*Institute of Physics, Academy of Sciences of the Czech Republic, Na Slovance 2, 182 21 Prague 8, Czech Republic*
[27]*Iowa State University, Ames, Iowa 50011, USA*
[28]*Advanced Science Research Center, Japan Atomic Energy Agency, 2-4 Shirakata Shirane, Tokai-mura, Naka-gun, Ibaraki-ken 319-1195, Japan*
[29]*Helsinki Institute of Physics and University of Jyväskylä, P.O.Box 35, FI-40014 Jyväskylä, Finland*
[30]*KEK, High Energy Accelerator Research Organization, Tsukuba, Ibaraki 305-0801, Japan*
[31]*Korea University, Seoul, 136-701, Korea*
[32]*Russian Research Center "Kurchatov Institute," Moscow, 123098 Russia*
[33]*Kyoto University, Kyoto 606-8502, Japan*
[34]*Laboratoire Leprince-Ringuet, Ecole Polytechnique, CNRS-IN2P3, Route de Saclay, F-91128, Palaiseau, France*
[35]*Physics Department, Lahore University of Management Sciences, Lahore 54792, Pakistan*
[36]*Lawrence Livermore National Laboratory, Livermore, California 94550, USA*
[37]*Los Alamos National Laboratory, Los Alamos, New Mexico 87545, USA*
[38]*Department of Physics, Lund University, Box 118, SE-221 00 Lund, Sweden*
[39]*University of Maryland, College Park, Maryland 20742, USA*
[40]*Department of Physics, University of Massachusetts, Amherst, Massachusetts 01003-9337, USA*
[41]*Department of Physics, University of Michigan, Ann Arbor, Michigan 48109-1040, USA*
[42]*Muhlenberg College, Allentown, Pennsylvania 18104-5586, USA*
[43]*Myongji University, Yongin, Kyonggido 449-728, Korea*
[44]*University of New Mexico, Albuquerque, New Mexico 87131, USA*
[45]*New Mexico State University, Las Cruces, New Mexico 88003, USA*
[46]*Department of Physics and Astronomy, Ohio University, Athens, Ohio 45701, USA*
[47]*Oak Ridge National Laboratory, Oak Ridge, Tennessee 37831, USA*
[48]*IPN-Orsay, Universite Paris Sud, CNRS-IN2P3, BP1, F-91406, Orsay, France*
[49]*PNPI, Petersburg Nuclear Physics Institute, Gatchina, Leningrad Region, 188300, Russia*
[50]*RIKEN Nishina Center for Accelerator-Based Science, Wako, Saitama 351-0198, Japan*
[51]*RIKEN BNL Research Center, Brookhaven National Laboratory, Upton, New York 11973-5000, USA*
[52]*Physics Department, Rikkyo University, 3-34-1 Nishi-Ikebukuro, Toshima, Tokyo 171-8501, Japan*
[53]*Saint Petersburg State Polytechnic University, St. Petersburg, 195251 Russia*
[54]*Department of Physics and Astronomy, Seoul National University, Seoul 151-742, Korea*
[55]*Chemistry Department, Stony Brook University, SUNY, Stony Brook, New York 11794-3400, USA*
[56]*Department of Physics and Astronomy, Stony Brook University, SUNY, Stony Brook, New York 11794-3800, USA*
[57]*University of Tennessee, Knoxville, Tennessee 37996, USA*
[58]*Department of Physics, Tokyo Institute of Technology, Oh-okayama, Meguro, Tokyo 152-8551, Japan*
[59]*Institute of Physics, University of Tsukuba, Tsukuba, Ibaraki 305, Japan*

[60] *Vanderbilt University, Nashville, Tennessee 37235, USA*
[61] *Weizmann Institute, Rehovot 76100, Israel*
[62] *Institute for Particle and Nuclear Physics, Wigner Research Centre for Physics, Hungarian Academy of Sciences (Wigner RCP, RMKI) H-1525 Budapest 114, POBox 49, Budapest, Hungary*
[63] *Yonsei University, IPAP, Seoul 120-749, Korea*
[64] *University of Zagreb, Faculty of Science, Department of Physics, Bijenička 32, HR-10002 Zagreb, Croatia*
(Dated: November 11, 2014)

We report on J/ψ production from asymmetric Cu+Au heavy-ion collisions at $\sqrt{s_{NN}}$=200 GeV at the Relativistic Heavy Ion Collider at both forward (Cu-going direction) and backward (Au-going direction) rapidities. The nuclear modification of J/ψ yields in Cu+Au collisions in the Au-going direction is found to be comparable to that in Au+Au collisions when plotted as a function of the number of participating nucleons. In the Cu-going direction, J/ψ production shows a stronger suppression. This difference is comparable in magnitude and has the same sign as the difference expected from shadowing effects due to stronger low-x gluon suppression in the larger Au nucleus.

PACS numbers: 25.75.Dw

* PHENIX Co-Spokesperson: morrison@bnl.gov
† PHENIX Co-Spokesperson: jamie.nagle@colorado.edu

I. INTRODUCTION

The long-standing goal of studying the production in high energy heavy ion collisions of $c\bar{c}$ bound states, known collectively as charmonium, has been to use the modification of their yield as a direct signal of deconfinement in the quark gluon plasma (QGP) [1–3]. Practically, the study of charmonium has been confined to the two lowest mass vector meson states, the strongly bound J/ψ and the much more weakly bound ψ'. In pursuit of this goal, the production of J/ψ has been studied at center of mass energies of $\sqrt{s_{_{NN}}} = 17.3$ GeV in Pb+Pb [4], In+In [5], and p+Pb [6, 7] collisions; at $\sqrt{s_{_{NN}}} = 19.4$ GeV in S+U collisions [8]; at $\sqrt{s_{_{NN}}} = 200$ GeV in p+p [9], d+Au [10, 11], Cu+Cu [12] and Au+Au [13, 14] collisions; and at $\sqrt{s_{_{NN}}} = 2.76$–7 TeV in p+p [15, 16], p+Pb [17] and Pb+Pb [18] collisions. Only one heavy ion on heavy ion collision system has asymmetric masses, S+U at 19.4 GeV, and that measurement was made at only one rapidity ($0<y<1$).

The studies of $p(d)$+A collisions at these and other energies were motivated by the need to understand cold nuclear matter (CNM) effects [2, 3]. These are effects that modify J/ψ production in a nuclear target in the absence of a QGP, and they are found to be very significant at all of these energies [6, 10, 17, 19–23]. CNM effects often considered include nuclear modification of the parton distributions in nuclei (nPDFs), break up of the J/ψ precursor $c\bar{c}$ state in the cold nucleus, nuclear transverse momentum broadening in traversing the cold nucleus, and initial state parton energy loss [2, 3]. It has been hoped that CNM effects and hot matter effects can be factorized, so that CNM effects can be measured in $p(d)$+A collisions and accounted for when analyzing heavy ion collision data to extract hot matter effects. This has not yet been clearly established.

The recent observation of what appears to be collective flow in p+Pb [24–26] and d+Au [27] collisions has called into question whether CNM effects are really isolated from hot matter effects in $p(d)$+A collisions. Evidence that J/ψ production is not modified by hot matter effects in $p(d)$+A collisions comes from the observation [28] that break up cross sections fitted to shadowing corrected J/ψ data from $p(d)$+A collisions at mid and backward rapidity scale with time spent in the nucleus across a broad range of collision energies. This observed scaling would presumably be broken if J/ψ production was modified by different hot matter effects at different collision energies. However unexpectedly strong suppression of the ψ' has been observed in both d+Au [29] and p+Pb [30] collisions, and so far this is unexplained. Since feed down from ψ' decays contributes only 10% to the J/ψ yield, it is possible that the weakly bound ψ' is sensitive to hot matter effects in $p(d)$+A collisions while the inclusive J/ψ yield is not.

There are additional data from $p(d)$+A collisions at lower collision energies [19–23]. Taken together with the $p(d)$+A data sets mentioned above, they cover a broad range of rapidities and $\sqrt{s_{_{NN}}}$ values. To try to shed some light on the nature of CNM effects on J/ψ production, these data have been described using models containing gluon shadowing/antishadowing plus break up of the charmonia precursor state by collisions with nucleons [7, 28, 31] and/or models of energy loss in cold nuclear matter [32, 33] or gluon saturation models [34]. A broad picture now seems to have emerged. The precursor to the fully formed charmonium is a $c\bar{c}$ state, formed primarily by gluon fusion, that becomes color neutral and expands to the final size of the meson on a time scale of a few tenths of a fm/c. When the proper time (in the $c\bar{c}$ frame) spent in the target nucleus is comparable with the charmonium formation time (which occurs at lower energies and at midrapidity, and at higher energies only at backward rapidities), the modification is well described by shadowing plus break up by nucleons [28]. When the time spent in the target nucleus is shorter than this (which occurs at higher energies, and at lower energies only at forward rapidity), the data are well described by models of shadowing plus energy loss or gluon saturation [32, 33]. Thus at RHIC energy ($\sqrt{s_{_{NN}}} = 200$ GeV) cold nuclear matter effects are believed to result from a variety of different mechanisms, and the mixture depends very strongly on rapidity.

Hot matter effects and CNM effects are present together in heavy ion collisions, and both are important. In Au+Au collisions at RHIC, for example, the addition of hot matter effects increases the suppression of the J/ψ by a factor of roughly two over what would be expected if only CNM effects were present [3, 13]. Moreover, in asymmetric mass collisions such as Cu+Au the distribution of final state energy is a function of rapidity [35], as reflected in the particle production. Thus hot matter effects will likely not be symmetric in rapidity. Cold nuclear matter effects will also be asymmetric in rapidity. First, the parton distribution functions are more strongly modified in the heavier Au nucleus. Forward rapidity (Cu-going) J/ψ production probes gluons at low Bjorken-x (*i.e.* low momentum fraction) in the Au nucleus, while in Cu the gluons at high Bjorken-x are probed. This is reversed for the backward rapidity (Au-going) J/ψ. Second, energy loss and breakup effects will be different in nuclei of different mass. In the case where the charmonium is emitted at forward rapidity it has a large rapidity relative to the Au nucleus, which it crosses in a very short proper time. At the same time, the J/ψ rapidity relative to the Cu nucleus is much smaller, and the crossing time is much larger. Because the different time scales lead to different mechanisms, energy loss effects will depend on the interaction between the charmonium precursor state and the Au nucleus, while breakup effects will depend on the interaction between the precursor and the Cu nucleus. For charmonium emitted at backward rapidity, this will be reversed. Thus the asymmetry in mass between Cu and Au will lead to asymmetric energy loss and breakup contributions at forward and backward rapidity. Forward versus backward rapidity J/ψ production in asymmetric

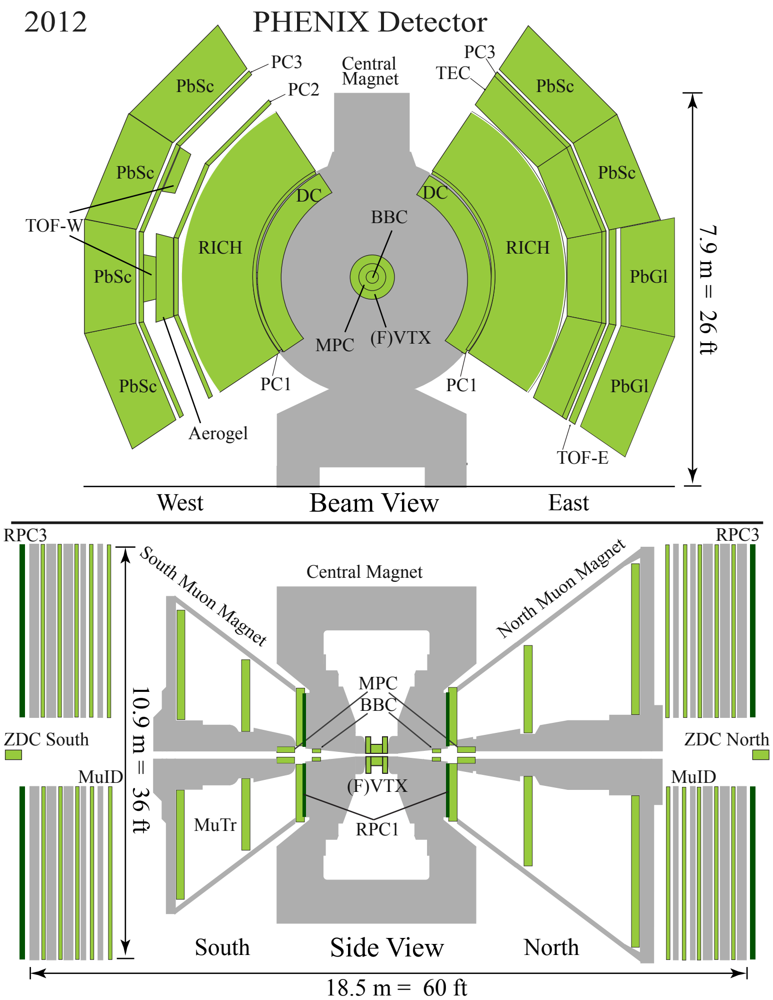

FIG. 1. (Color online) A schematic side view of the PHENIX detector configuration for the 2012 run.

mass collisions will therefore contain different contributions from both hot matter effects and CNM effects. There are also simple geometric models separating core-corona contributions that would be useful to confront with data in central Cu+Au [36]. The comparison of d+Au, Au+Au and Cu+Au J/ψ modifications across rapidities may provide key insight on the balance of cold and hot nuclear matter effects, and whether they are truly factorizable.

A heavy ion collision system with asymmetric masses, Cu+Au, was studied experimentally for the first time at RHIC in the 2012 run. In this paper we present nuclear modification data from the PHENIX experiment on J/ψ production in Cu+Au collisions at $\sqrt{s_{NN}}$ = 200 GeV at two rapidities, $-2.2<y<-1.2$ and $1.2<y<2.2$.

II. PHENIX DETECTOR

The PHENIX detector recorded Cu+Au events at $\sqrt{s_{NN}} = 200\,$GeV during the 2012 data-taking period at the Relativistic Heavy-Ion Collider (RHIC) at Brookhaven National Laboratory. The detector is shown schematically in Fig. 1. Global event information is obtained from the beam-beam counters (BBC), which comprise two arrays of 64 quartz Čerenkov counters that measure charged particles within the pseudorapidity range ($3.0<|\eta|<3.9$). The BBC provides the primary level-1 trigger for Cu+Au minimum bias events, requiring two or more hits on each side of the interaction point and a fast reconstructed event vertex located along the beam direction within $\pm30\,$cm of the nominal center of the PHENIX acceptance. For this analysis, 20.7 billion ($\mathcal{L} = 4.3\,\mathrm{nb}^{-1}$) sampled minimum bias events were used within $\pm30\,$cm. The corresponding N+N integrated luminosity used is $53\,\mathrm{pb}^{-1}$.

For the data set used in this analysis the primary level-1 trigger from the BBC is required to be in coincidence

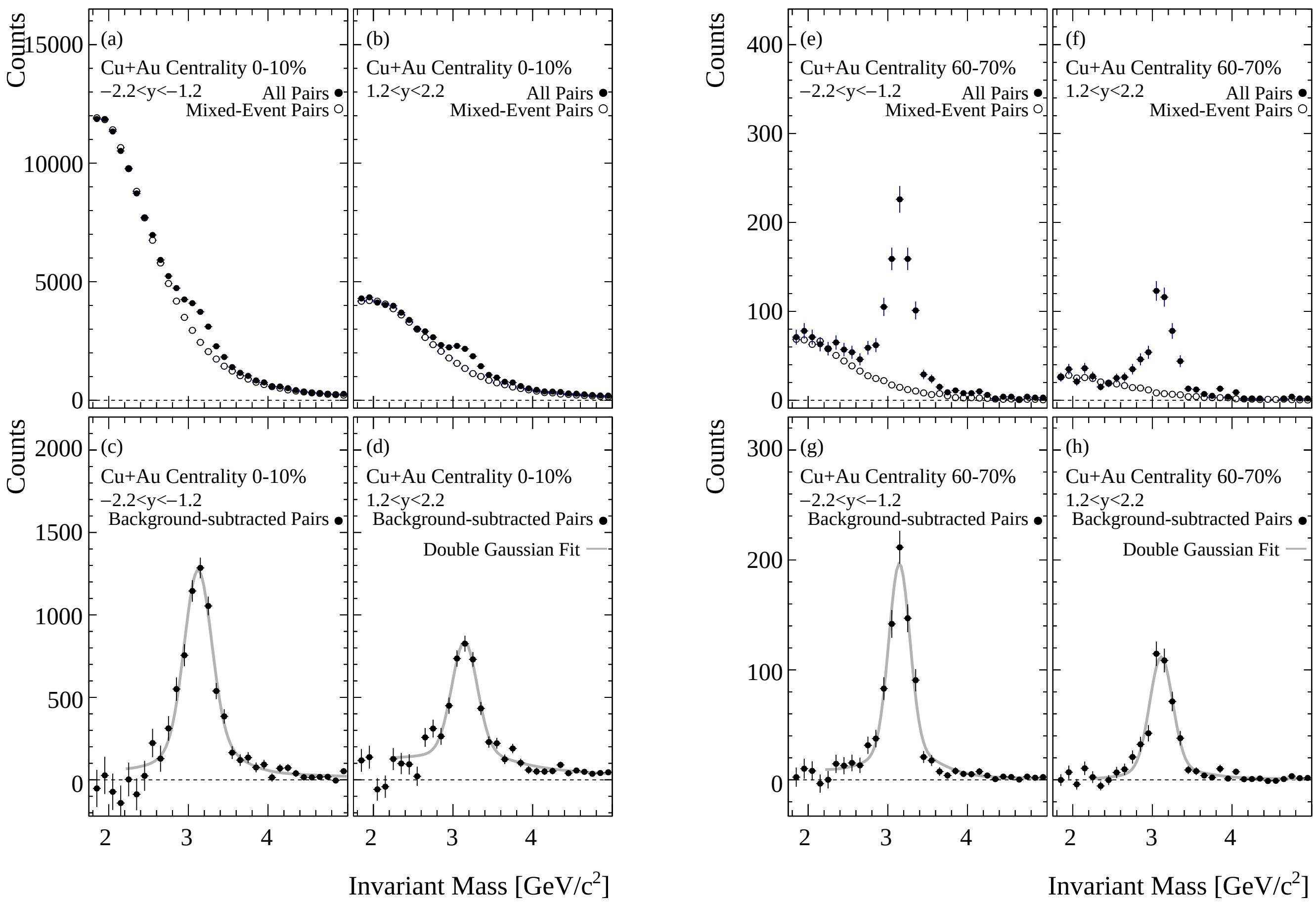

FIG. 2. Dimuon invariant mass spectra measured in central 0%–10% (left panels (a)–(d)) and mid-peripheral (60%–70%) (right panels ((e)–(h)) collisions integrated over the full p_T range. In each figure, the top panels ((a),(b),(e), and (f)) show the distribution of invariant mass, reconstructed from all same-event opposite charge-sign pairs (filled symbols) and mixed-event pairs (open symbols) in Cu+Au collisions. The lower panels ((c),(d),(g), and (h)) show the combinatorial background subtracted pairs from the upper panels. For the 0%–10% (60%–70%) data, panels (a) and (c) ((e) and (g)) show pairs reconstructed in the backward (-2.2<y<-1.2) and panels (b) and (d) ((f) and (h)) forward (1.2<y<2.2) muons arms respectively. The solid line represents a fit to the data using a double Gaussian line shape plus an exponential background, see text for details.

with an additional level-1 trigger, requiring two muon candidates to penetrate fully through the muon identifier. The trigger logic for a muon candidate requires a road of fired Iarocci tubes in at least four planes, including the most downstream plane relative to the collision point.

Muons at forward rapidities are reconstructed in this analysis using the South and North (see Fig. 1) muon spectrometers. The muon spectrometers comprise four sub-components: a steel absorber, a magnet (one per spectrometer), a muon tracker (MuTr), and a muon identifier (MuID). A detailed description of the muon detectors is given in [37]. In 2010, an additional 36.2 cm of steel absorbers ($\lambda_I = 2.3$) were added to help increase the relative yield of muons compared to hadronic background. This additional material decreases the efficiency of the low-p_T muons which punch through all muon arm materials by ∼30%–40%. The minimum momentum for a muon to reach the outermost MuID plane is 3 GeV/c. Three sets of cathode strip chambers (MuTr), inside the muon magnet, follow the absorber material which are used to measure the momentum of tracks within the detector volume. The final component (MuID) comprises alternating steel absorbers and Iarocci tubes, which further reduce the number of hadronic tracks which punch through the initial layers of absorber material and masquerade as muons.

III. DATA ANALYSIS

A. Centrality Determination

The events are sorted into centrality classes using the combined charge from both BBC counters. The number of participating nucleons ($N_{\rm part}$) and number of binary collisions ($N_{\rm coll}$) in each centrality class is obtained from a Monte Carlo Glauber calculation [38] folded with a Negative Binomial Distribution that is fitted to the measured BBC charge distribution in the charge range where the BBC trigger is fully efficient. For peripheral events where the minimum bias trigger is not fully efficient, the efficiency is obtained from a comparison of the measured BBC charge distribution to the Negative Binomial Distribution. The minimum bias trigger is determined to fire on $93\% \pm 3\%$ of the inelastic Cu+Au cross section.

Several baseline parameters are used to characterize the Glauber model nuclei and their interactions. Nucleons in each gold and copper nucleus are distributed using a Woods-Saxon function, given in Eq. 1, with a radius, R, of 6.38 fm (Au) and 4.20 fm (Cu) along with diffuseness, a, of 0.535 fm and 0.596 fm respectively. A minimum internucleon distance is enforced to be 0.4 fm (known as the hard-core radius) such that nucleons cannot overlap in the nucleus. The nucleon-nucleon inelastic scattering cross section of 42 mb is used as default.

$$\rho(r) = \frac{\rho_0}{1 + e^{-(R-r)/a}} \tag{1}$$

The systematic uncertainties on $N_{\rm part}$ and $N_{\rm coll}$ are estimated by varying the baseline parameters to the Glauber model from four sources:

1. The nucleon-nucleon inelastic scattering cross section of 42 mb is varied by ± 3 mb.
2. Extreme radii and diffuseness cases were compared to the default baseline using (a) $R_{\rm Au} = 6.25$ fm, $a_{\rm Au} = 0.530$ fm and $R_{\rm Cu} = 4.11$ fm, $a_{\rm Cu} = 0.590$ fm, and (b) $R_{\rm Au} = 6.65$ fm, $a_{\rm Au} = 0.550$ fm and $R_{\rm Cu} = 4.38$ fm, $a_{\rm Cu} = 0.613$ fm.
3. The condition of a minimum internucleon distance was removed such that nucleons are allowed to overlap in the initial nucleon distribution.
4. Since the trigger efficiency is 93% with an uncertainty of 3%, the Glauber parameters are also calculated assuming an efficiency of 90% and 96%.

A total of eight variations (including the baseline) of the Glauber model conditions are used to estimate the systematic uncertainties. The extracted total cross section from this Glauber model for Cu+Au collisions is estimated to be $\sigma_{\rm Cu+Au} = 5.23 \pm 0.15\, b$. The results are summarized in Table I.

TABLE I. Glauber-estimated centrality parameters in Cu+Au collisions.

Centrality	$N_{\rm coll}$	$N_{\rm part}$	$N_{\rm part}^{Au}$	$N_{\rm part}^{Cu}$
0%–10%	373.3 ± 34.6	177.2 ± 5.2	117.5 ± 3.4	59.7 ± 1.8
10%–20%	254.2 ± 21.7	132.4 ± 3.7	82.1 ± 2.3	50.2 ± 1.4
20%–30%	161.5 ± 14.8	95.1 ± 3.2	56.8 ± 1.9	38.3 ± 1.3
30%–40%	97.1 ± 10.1	65.7 ± 3.4	38.3 ± 2.0	27.5 ± 1.4
40%–50%	55.0 ± 6.3	43.3 ± 3.0	24.8 ± 1.7	18.5 ± 1.3
50%–60%	29.0 ± 3.9	26.8 ± 2.6	15.1 ± 1.5	11.7 ± 1.2
60%–70%	14.0 ± 2.4	15.2 ± 2.0	8.5 ± 1.1	6.8 ± 0.9
70%–80%	6.2 ± 1.4	7.9 ± 1.5	4.3 ± 0.8	3.5 ± 0.7
80%–90%	2.4 ± 0.7	3.6 ± 0.8	1.9 ± 0.4	1.7 ± 0.4

B. Muon-Track Reconstruction

The data reported here were obtained from the PHENIX muon spectrometers, which cover the rapidity ranges $-2.2<y<-1.2$ and $1.2<y<2.2$. Muon candidates are reconstructed by finding tracks that penetrate through all layers of the MuID, then matching these to tracks in the MuTr. The requirement of the track penetrating the full absorber material through the MuID significantly reduces the hadron contribution. However, with small probability (of order $\sim$1/1000) a charged hadron may penetrate the material without suffering a hadronic interaction. Additionally, the muon spectrometer cannot reject most muons that originate from charged pions and kaons which decay before the absorber in front of the MuTr. For the dimuon reconstruction in this analysis, pairs of muon candidate tracks are selected and a combined fit is performed with the collision z-vertex from the BBC. We apply various cuts to enhance the sample of good muon track pairs, including cuts on the individual track χ^2 values, the matching between position and direction vectors of the MuID track and the MuTr track projected to the front of the MuID, and finally the χ^2 of the track pair and BBC z-vertex combined fit.

C. μ^++μ^- Analysis

All opposite charge-sign pairs within an event are combined to form an effective invariant mass, see Fig. 2. Punch-through hadrons or single muons can randomly combine to form a combinatorial background. Muon pairs from decays of heavy vector-mesons, the ψ and Υ families, form peaks in the mass spectrum. There are continuum contributions from correlated muon pairs due to the Drell-Yan process, and due to correlated semileptonic open heavy flavor decays. Owing to the momentum resolution in the MuTr, distinct J/ψ and ψ' peaks are not visible in this analysis. The left and right panels represent data in the most central event class (0%–10%) and a mid-peripheral (60%–70%) class respectively.

The total combinatorial background is estimated using a mixed event technique, where oppositely charged tracks from different events are combined to form an effective mass (see [13] for details). As these are independent events, all real correlations are necessarily absent and only the combinatorial background remains (open symbols on the upper panels of Fig. 2). The combinatorial background is normalized using like-sign yields found in both the mixed-pairs and real-pairs data samples in a range close to the J/ψ mass peak region, 2.6<mass<3.6 GeV/c^2, using a similar procedure as [13]. The found normalization constant is varied by $\pm$2% and is included in the systematic uncertainty. To extract the yield, a fit is made which includes the normalized combinatorial background (from above) plus an acceptance-modified [9] double-Gaussian line shape which represents the J/ψ signal, along with an acceptance-modified exponential term to account for the remaining correlated physical background. The double-Gaussian line shape is inspired by the line shape measured in p+p collisions [39], only the yield and the J/ψ mass width are allowed to vary, the latter accounts for its degradation in the large background of heavy-ion collisions. The resultant mass width is found to vary linearly with multiplicity in the spectrometer arms from 0.15 GeV/c^2 at low multiplicity to 0.18 GeV/c^2 at the highest multiplicity in Cu+Au collisions. The fit range is from 1.75 to 5.0 GeV/c^2, and the resultant fit function is shown as a solid line on Fig 2. Systematic uncertainties of 2.2%-10.6% (see Table II) are associated with the yield extraction to account for uncertainty in the combinatorial background subtraction and the fit function and fit range used. Additionally, the extracted yields were systematically checked for consistency by using both a like-sign combinatorial fit and a bin-counting method. The yields are found to agree within the statistical uncertainty. A total of 35k J/ψ are counted across all centrality and rapidities.

D. Efficiency and Corrections

The efficiency for reconstructing the J/ψ in the muon arms is estimated by embedding PYTHIA 5.428 [40] $J/\psi \to \mu^+\mu^-$ into real minimum bias events (i.e. a sample of events which do not necessarily contain a J/ψ candidate). First, the PYTHIA $J/\psi \to \mu^+\mu^-$ events are simulated through a full GEANT 3.21 [41] description of the PHENIX detector. This simulation accounts for inefficiencies due to dead materials, including those due to the additional steel absorber. The resultant simulated hits in the muon tracker and identifier are added to the signals found in the real data event. Once embedded, the amalgamated event is passed through the same full reconstruction chain as used for real data. The simulations include a trigger emulator. In the final step, the yield of reconstructed J/ψ divided by the originally simulated number of PYTHIA $J/\psi \to \mu^+\mu^-$, in the same rapidity range, determines the acceptance×efficiency correction factor ($A\epsilon$ in Eq. 2). Depending on which muon spectrometer and the centrality, the acceptance×efficiency varies from 2.5% (3.6%) (0%–10% central at positive (negative) rapidity) to 3.4% (5.2%) (70%–80% peripheral).

Uncertainties due to the assumed input PYTHIA rapidity and momentum distributions for the $J/\psi \to \mu^+\mu^-$ were previously evaluated for the correction factors and were found to be $\sim$4% [42]. An efficiency uncertainty of $\sim$10% represents an overall uncertainty on extracting the reconstruction and trigger efficiency from the embedding procedure. Small run-to-run variations in the detector acceptance and MuID efficiencies were also evaluated to be 5% and 2.8%, respectively. These systematic uncertainties are added in quadrature for the total uncertainty on the measured yields.

An error representing the uncertainty in determining the efficiency (10%) is also added in quadrature to the Type-B systematic uncertainty.

TABLE II. Estimated systematic uncertainties.

Source	Uncertainty (%)	Type
J/ψ Signal extraction	±2.2–10.6	A
run-to-run efficiency variation	±2.8	B
Input J/ψ p_T distributions	±4.0	B
Detector acceptance	±5.0	B
Reconstruction and trigger efficiency	±10.0	B
Glauber (N_{coll})	±10–29	B
p+p reference	±7.1	C

The invariant J/ψ yields ($\frac{dN}{dy}$) are calculated for the $J/\psi \to \mu^+\mu^-$ branching fraction, B, from

$$B\frac{dN}{dy} = \frac{1}{N_{\mathrm{event}}}\frac{N^{J\psi}_{\mathrm{measured}}}{\Delta y A\epsilon} \tag{2}$$

$N^{J/\psi}_{\mathrm{measured}}$ is the number of measured J/ψ per unit rapidity (Δy), integrated over all transverse momenta. The detector has good acceptance at all values of p_T, including zero, due to the boost of daughter muons at forward and backward rapidity. The number of minimum-bias equivalent events is given by N_{event}.

IV. RESULTS

The invariant yields calculated using Eq. 2 are summarized in Table III. The nuclear modification factor, R_{AA} is formed from the invariant yields using Eq. 3,

$$R_{AA} = \frac{1}{\langle N_{\mathrm{coll}}\rangle}\frac{dN(\mathrm{CuAu})/dy}{dN(pp)/dy}, \tag{3}$$

where $dN(\mathrm{CuAu})/dy$ and $dN(pp)/dy$ represent the invariant yields measured in Cu+Au and p+p collisions, respectively. Data from the same detector recorded in 2006 and 2008 are used as the reference p+p data [10].

TABLE III. Invariant yield at forward (1.2<y<2.2) and backward (-2.2<y<-1.2) rapidity as a function of centrality. The first and second uncertainties listed represent Type-A and Type-B uncertainties, respectively (see text for definitions). No Type-C (global) systematic is assigned.

Centrality	$B\frac{dN}{dy} \times 10^{-6}$ Forward Cu-going direction 1.2<y<2.2	Backward Au-going direction -2.2<y<-1.2
0%–10%	$60.53 \pm 6.39 \pm 7.39$	$68.76 \pm 3.16 \pm 8.39$
10%–20%	$46.99 \pm 4.53 \pm 5.74$	$60.12 \pm 2.56 \pm 7.34$
20%–30%	$31.50 \pm 2.80 \pm 3.85$	$43.31 \pm 2.97 \pm 5.29$
30%–40%	$22.05 \pm 1.28 \pm 2.69$	$29.25 \pm 1.28 \pm 3.57$
40%–50%	$16.45 \pm 0.94 \pm 2.01$	$19.96 \pm 0.95 \pm 2.44$
50%–60%	$9.92 \pm 0.57 \pm 1.21$	$11.95 \pm 0.80 \pm 1.46$
60%–70%	$5.76 \pm 0.40 \pm 0.70$	$6.80 \pm 0.32 \pm 0.83$
70%–80%	$3.52 \pm 0.28 \pm 0.43$	$3.68 \pm 0.30 \pm 0.45$
80%–90%	$1.44 \pm 0.20 \pm 0.18$	$1.59 \pm 0.14 \pm 0.19$

TABLE IV. Nuclear modification factor (R_{AA}) at forward ($1.2<y<2.2$ – Cu-going) and backward ($-2.2<y<-1.2$ – Au-going) rapidity and forward/backward ratio as a function of centrality. The first and second uncertainties listed represent Type-A and Type-B uncertainties, respectively (see text for definitions). An additional 7.1% Type-C (global) systematic also applies for the R_{AA}.

Centrality	R_{AA} Forward Cu-going direction $1.2<y<2.2$	R_{AA} Backward Au-going direction $-2.2<y<-1.2$	Forward/Backward Ratio
0%–10%	0.239 ± 0.025 ± 0.037	0.271 ± 0.012 ± 0.042	0.88 ± 0.10 ± 0.14
10%–20%	0.272 ± 0.026 ± 0.040	0.348 ± 0.015 ± 0.052	0.78 ± 0.08 ± 0.13
20%–30%	0.287 ± 0.026 ± 0.044	0.394 ± 0.027 ± 0.060	0.73 ± 0.08 ± 0.12
30%–40%	0.334 ± 0.019 ± 0.054	0.443 ± 0.019 ± 0.071	0.75 ± 0.05 ± 0.12
40%–50%	0.440 ± 0.025 ± 0.074	0.534 ± 0.025 ± 0.089	0.82 ± 0.06 ± 0.13
50%–60%	0.486 ± 0.028 ± 0.087	0.586 ± 0.039 ± 0.104	0.83 ± 0.07 ± 0.14
60%–70%	0.605 ± 0.042 ± 0.127	0.714 ± 0.034 ± 0.150	0.85 ± 0.07 ± 0.14
70%–80%	0.835 ± 0.065 ± 0.214	0.873 ± 0.072 ± 0.224	0.96 ± 0.11 ± 0.16
80%–90%	0.875 ± 0.124 ± 0.268	0.968 ± 0.084 ± 0.296	0.90 ± 0.15 ± 0.15

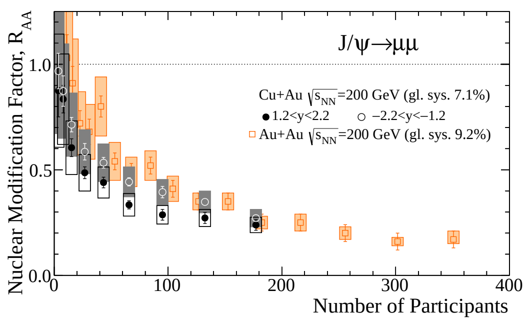

FIG. 3. (Color online) Nuclear modification factor, R_{AA}, measured as a function of collision centrality (N_{part}). Values for J/ψ at forward (Cu-going) rapidity are shown as closed circles and at backward (Au-going) rapidity as open circles. For reference, Au+Au data [13] are also shown, averaged over forward and backward rapidities, as red squares.

The values of R_{AA} versus centrality are listed in Table IV and shown as a function of N_{part} in Fig. 3. The R_{AA} for Au+Au collisions [13] at the same collision energy and rapidity (red squares) is shown in Fig. 3 for comparison. The dependence of the Cu+Au nuclear modification on N_{part} at backward (Au-going) rapidity is similar to that for Au+Au collisions, while the Cu+Au R_{AA} at forward (Cu-going) rapidity is noticeably lower.

The uncertainties on the measured yield values are separated into three types. Type-A uncertainties are random point-to-point uncertainties which are combined in quadrature with the statistical uncertainty associated with each data point. These are represented by vertical bars in the figures. Type-B uncertainties are correlated point-to-point systematic uncertainties which are represented by boxes in the figures. Type-C uncertainties represent a global systematic scale uncertainty, which represents the scale uncertainty from the measured p+p reference data. The values of the point-to-point systematic uncertainties are summarized in Table II.

Forward and backward differences can be observed when forming the ratio of the yield values for the forward rapidity to the backward rapidity. This is shown in Fig. 4, and the values are presented in Table IV. This ratio

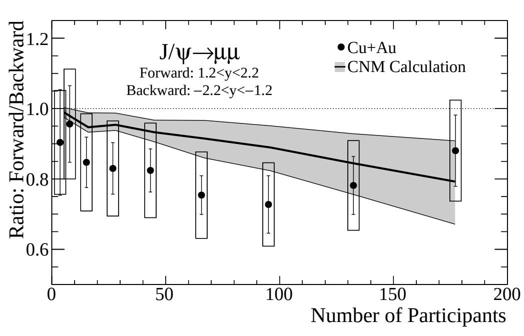

FIG. 4. Ratio of forward- to backward-rapidity (Cu-going/Au-going) J/ψ yields measured in Cu+Au collisions (symbols). Also shown is a model [43] which estimates the contribution from cold nuclear matter; the band represents the extreme nPDF parameter sets as described in [44].

has the advantage of reduced systematic uncertainties due to the cancellation of type-C and some type-B correlated uncertainties that apply to R_{AA}, those which are related to the Glauber model calculation. The 20%–30% difference in suppression between forward and backward rapidity R_{AA} evident in Fig. 4 could be due to hot matter effects, CNM effects, or a combination of both.

To obtain an indication of the expected size of the difference due to CNM effects, we use a simple Glauber model that combines gluon modifications as a function of Bjorken x and Q^2, taken from the EPS09 shadowing parametrization [44], and a single effective $c\bar{c}$ break up cross section (4 mb) that approximately reproduces the d+Au nuclear modification observed in PHENIX data across all rapidities [43]. It should be emphasized that this simple model uses a constant effective $c\bar{c}$ cross section to account for nonshadowing effects at all rapidities, while in fact both breakup and energy loss contributions are expected to be rapidity dependent. Thus the calculation reflects only the expected difference in shadowing between forward and backward rapidity in Cu+Au. The calculation, shown in Fig. 4 indicates that the size of the expected shadowing difference is comparable with the effect seen in the data, and has the same sign.

Hot matter effects are expected to be greater at backward rapidity in Cu+Au collisions, where the particle multiplicity for central collisions should be about 20% higher in the Au-going direction than in the Cu-going direction [35]. In contrast, the asymmetry of the number of participating nucleons in the Au-going direction more rapidly increases compared to Cu-going participants, with twice as many in central collisions. This disparity prohibits the interpretation of scaling properties due directly to hot matter effects, without further theroretical input. However, increased suppression due to higher energy density at backward rapidity would lead to an increase in the ratio shown in Fig. 4. Increased recombination effects may also occur at higher energy density (see for example [45]), increasing the J/ψ yield and tending to decrease the ratio shown in Fig. 4.

The new rapidity dependent Cu+Au J/ψ data presented here form part of a large J/ψ data set at RHIC energies that includes p+p, d+Au, Cu+Cu and Au+Au collision data. These J/ψ nuclear modification data result from a varied mix of energy densities and cold nuclear matter effects, providing a broad range of conditions with which to confront models of J/ψ production.

V. SUMMARY AND CONCLUSIONS

We have measured the centrality dependence of J/ψ production in asymmetric Cu+Au collisions. We find the centrality evolution of the nuclear modification (R_{AA}) at backward rapidity to be similar to that measured in Au+Au collisions at the same number of participants, while at forward rapidity (the Cu-going direction) it is significantly smaller. At backward rapidity, in the most central 10% collisions, $R_{AA} = 0.271 \pm 0.012 \pm 0.042$. At forward rapidity the suppression is on average about 20% stronger in the centrality range 0%–40%, while for the most peripheral collisions the ratio is consistent with unity within systematic uncertainties.

The difference between forward (Cu-going) and backward (Au-going) J/ψ modification is found to be comparable in magnitude and of the same sign as the expected difference from shadowing effects. These data add a completely new admixture of hot and cold nuclear matter effects to those already sampled for J/ψ production at RHIC energies, broadening the range of conditions with which models of J/ψ production can be confronted.

ACKNOWLEDGMENTS

We thank the staff of the Collider-Accelerator and Physics Departments at Brookhaven National Laboratory and the staff of the other PHENIX participating institutions for their vital contributions. We acknowledge support from the Office of Nuclear Physics in the Office of Science of the Department of Energy, the National Science Foundation, Abilene Christian University Research Council, Research Foundation of SUNY, and Dean of the College of Arts and Sciences, Vanderbilt University (U.S.A), Ministry of Education, Culture, Sports, Science, and Technology and the Japan Society for the Promotion of Science (Japan), Conselho Nacional de Desenvolvimento Científico e Tecnológico and Fundação de Amparo à Pesquisa do Estado de São Paulo (Brazil), Natural Science Foundation of China (P. R. China), Ministry of Science, Education, and Sports (Croatia), Ministry of Education, Youth and Sports (Czech Republic), Centre National de la Recherche Scientifique, Commissariat à l'Énergie Atomique, and Institut National de Physique Nucléaire et de Physique des Particules (France), Bundesministerium für Bildung und Forschung, Deutscher Akademischer Austausch Dienst, and Alexander von Humboldt Stiftung (Germany), Hungarian National Science Fund, OTKA (Hungary), Department of Atomic Energy and Department of Science and Technology (India), Israel Science Foundation (Israel), National Research Foundation of Korea of the Ministry of Science, ICT, and Future Planning (Korea), Physics Department, Lahore University of Management Sciences (Pakistan), Ministry of Education and Science, Russian Academy of Sciences, Federal Agency of Atomic Energy (Russia), VR and Wallenberg Foundation

(Sweden), the U.S. Civilian Research and Development Foundation for the Independent States of the Former Soviet Union, the Hungarian American Enterprise Scholarship Fund, and the US-Israel Binational Science Foundation.

[1] T. Matsui and H. Satz, Phys. Lett. B **178**, 416 (1986).
[2] A. D. Frawley, T. Ullrich, and R. Vogt, Phys. Rept. **462**, 125 (2008).
[3] N. Brambilla, S. Eidelman, B. K. Heltsley, R. Vogt, G. T. Bodwin, *et al.*, Eur. Phys. J. C **71**, 1534 (2011).
[4] B. Alessandro *et al.* (NA50 Collaboration), Eur. Phys. J. C **39**, 335 (2005).
[5] R. Arnaldi *et al.* (NA60 Collaboration), Phys. Rev. Lett. **99**, 132302 (2007).
[6] R. Arnaldi *et al.* (NA60 Collaboration), Phys. Lett. B **706**, 263 (2012).
[7] R. Arnaldi (NA60 Collaboration), Nucl. Phys. A **830**, 345C (2009).
[8] M. Abreu *et al.* (NA50 Collaboration), Phys. Lett. B **466**, 408 (1999).
[9] A. Adare *et al.* (PHENIX Collaboration), Phys. Rev. D **85**, 092004 (2012).
[10] A. Adare *et al.* (PHENIX Collaboration), Phys. Rev. Lett. **107**, 142301 (2011).
[11] A. Adare *et al.* (PHENIX Collaboration), Phys. Rev. C **87**, 034904 (2013).
[12] A. Adare *et al.* (PHENIX Collaboration), Phys. Rev. Lett. **101**, 122301 (2008).
[13] A. Adare *et al.* (PHENIX Collaboration), Phys. Rev. C **84**, 054912 (2011).
[14] A. Adare *et al.* (PHENIX Collaboration), Phys. Rev. Lett. **98**, 232301 (2007).
[15] B. Abelev *et al.* (ALICE Collaboration), Phys. Lett. B **718**, 295 (2012).
[16] K. Aamodt *et al.* (ALICE Collaboration), Phys. Lett. B **704**, 442 (2011).
[17] B. B. Abelev *et al.* (ALICE Collaboration), (), arXiv:1308.6726.
[18] B. B. Abelev *et al.* (ALICE Collaboration), (), arXiv:1311.0214.
[19] M. Leitch *et al.* (FNAL E866/NuSea Collaboration), Phys. Rev. Lett. **84**, 3256 (2000).
[20] I. Abt *et al.* (HERA-B Collaboration), Eur. Phys. J. C **60**, 525 (2009).
[21] J. Badier *et al.* (NA3 Collaboration), Z. Phys. C **20**, 101 (1983).
[22] B. Alessandro *et al.* (NA50 Collaboration), Eur. Phys. J. C **33**, 31 (2004).
[23] B. Alessandro *et al.* (NA50 Collaboration), Eur. Phys. J. C **48**, 329 (2006).
[24] B. Abelev *et al.* (ALICE Collaboration), Phys. Lett. B **719**, 29 (2013).
[25] G. Aad *et al.* (ATLAS Collaboration), Phys. Lett. B **725**, 60 (2013).
[26] S. Chatrchyan *et al.* (CMS Collaboration), Phys. Lett. B **724**, 213 (2013).
[27] A. Adare *et al.* (PHENIX Collaboration), Phys. Rev. Lett. **111**, 212301 (2013).
[28] D. McGlinchey, A. D. Frawley, and R. Vogt, Phys. Rev. C **87**, 054910 (2013).
[29] A. Adare *et al.* (PHENIX Collaboration), Phys. Rev. Lett. **111**, 202301 (2013).
[30] M. Winn *et al.*, (ALICE Collaboration) unpublished.
[31] C. Lourenço, R. Vogt, and H. K. Wöhri, J. High Energy Phys. **02 (2009)** 014.
[32] F. Arleo and S. Peigne, ArXiv:1212.0434.
[33] F. Arleo, R. Kolevatov, S. Peigne, and M. Rustamova, J. High Energy Phys. **05 (2013)** 155.
[34] D. Kharzeev and K. Tuchin, Nucl. Phys. A **770**, 40 (2006).
[35] L.-W. Chen and C. M. Ko, Phys. Rev. C **73**, 014906 (2006).
[36] S. Digal, H. Satz, and R. Vogt, Phys. Rev. C **85**, 034906 (2012).
[37] H. Akikawa *et al.*, Nucl. Instrum. Methods A **449**, 537 (2003).
[38] M. L. Miller, K. Reygers, S. J. Sanders, and P. Steinberg, Ann. Rev. Nucl. Part. Sci. **57**, 205 (2007).
[39] A. Adare *et al.* (PHENIX Collaboration), Phys. Rev. C **77**, 024912 (2008).
[40] T. Sjostrand, S. Mrenna, and P. Skands, "Pythia 6.4 physics and manual," J. High Energy Phys. **05 (2006)** 026.
[41] *GEANT 3.2.1*, *GEANT 3.2.1*, CERN Program Library (1994), `http://wwwasdoc.web.cern.ch/wwwasdoc/pdfdir/geant.pdf`.
[42] A. Adare *et al.* (PHENIX Collaboration), Phys. Rev. C **86**, 064901 (2012).
[43] J. L. Nagle, A. D. Frawley, L. A. Linden Levy, and M. G. Wysocki, Phys. Rev. C **84**, 044911 (2011).
[44] K. J. Eskola, H. Paukkunen, and C. A. Salgado, J. High Energy Phys. **04 (2009)** 065.
[45] X. Zhao and R. Rapp, Phys. Rev. C **82**, 064905 (2010).